Studies of $X(3872)$ and $\psi(2S)$ production in $p\bar{p}$ collisions at 1.96 TeV

V. M. Abazov,[31] B. Abbott,[67] B. S. Acharya,[25] M. Adams,[46] T. Adams,[44] J. P. Agnew,[41] G. D. Alexeev,[31] G. Alkhazov,[35] A. Alton,[56,b] A. Askew,[44] S. Atkins,[54] K. Augsten,[7] V. Aushev,[38] Y. Aushev,[38] C. Avila,[5] F. Badaud,[10] L. Bagby,[45] B. Baldin,[45] D. V. Bandurin,[74] S. Banerjee,[25] E. Barberis,[55] P. Baringer,[53] J. F. Bartlett,[45] U. Bassler,[15] V. Bazterra,[46] A. Bean,[53] M. Begalli,[2] L. Bellantoni,[45] S. B. Beri,[23] G. Bernardi,[14] R. Bernhard,[19] I. Bertram,[39] M. Besançon,[15] R. Beuselinck,[40] P. C. Bhat,[45] S. Bhatia,[58] V. Bhatnagar,[23] G. Blazey,[47] S. Blessing,[44] K. Bloom,[59] A. Boehnlein,[45] D. Boline,[64] E. E. Boos,[33] G. Borissov,[39] M. Borysova,[38,c] A. Brandt,[71] O. Brandt,[20] M. Brochmann,[75] R. Brock,[57] A. Bross,[45] D. Brown,[14] X. B. Bu,[45] M. Buehler,[45] V. Buescher,[21] V. Bunichev,[33] S. Burdin,[39,d] C. P. Buszello,[37] E. Camacho-Pérez,[28] B. C. K. Casey,[45] H. Castilla-Valdez,[28] S. Caughron,[57] S. Chakrabarti,[64] K. M. Chan,[51] A. Chandra,[73] E. Chapon,[15] G. Chen,[53] S. W. Cho,[27] S. Choi,[27] B. Choudhary,[24] S. Cihangir,[45,a] D. Claes,[59] J. Clutter,[53] M. Cooke,[45,e] W. E. Cooper,[45] M. Corcoran,[73,a] F. Couderc,[15] M.-C. Cousinou,[12] J. Cuth,[21] D. Cutts,[70] A. Das,[72] G. Davies,[40] S. J. de Jong,[29,30] E. De La Cruz-Burelo,[28] F. Déliot,[15] R. Demina,[63] D. Denisov,[65] S. P. Denisov,[34] S. Desai,[45] C. Deterre,[41,f] K. DeVaughan,[59] H. T. Diehl,[45] M. Diesburg,[45] P. F. Ding,[41] A. Dominguez,[59] A. Drutskoy,[32,g] A. Dubey,[24] L. V. Dudko,[33] A. Duperrin,[12] S. Dutt,[23] M. Eads,[47] D. Edmunds,[57] J. Ellison,[43] V. D. Elvira,[45] Y. Enari,[14] H. Evans,[49] A. Evdokimov,[46] V. N. Evdokimov,[34] A. Fauré,[15] L. Feng,[47] T. Ferbel,[63] F. Fiedler,[21] F. Filthaut,[29,30] W. Fisher,[57] H. E. Fisk,[45] M. Fortner,[47] H. Fox,[39] J. Franc,[7] S. Fuess,[45] P. H. Garbincius,[45] A. Garcia-Bellido,[63] J. A. García-González,[28] V. Gavrilov,[32] W. Geng,[12,57] C. E. Gerber,[46] Y. Gershtein,[60] G. Ginther,[45] O. Gogota,[38] G. Golovanov,[31] P. D. Grannis,[64] S. Greder,[16] H. Greenlee,[45] G. Grenier,[17] Ph. Gris,[10] J.-F. Grivaz,[13] A. Grohsjean,[15,f] S. Grünendahl,[45] M. W. Grünewald,[26] T. Guillemin,[13] G. Gutierrez,[45] P. Gutierrez,[67] J. Haley,[68] L. Han,[4] K. Harder,[41] A. Harel,[63] J. M. Hauptman,[52] J. Hays,[40] T. Head,[41] T. Hebbeker,[18] D. Hedin,[47] H. Hegab,[68] A. P. Heinson,[43] U. Heintz,[70] C. Hensel,[1] I. Heredia-De La Cruz,[28,h] K. Herner,[45] G. Hesketh,[41,i] M. D. Hildreth,[51] R. Hirosky,[74] T. Hoang,[44] J. D. Hobbs,[64] B. Hoeneisen,[9] J. Hogan,[73] M. Hohlfeld,[21] J. L. Holzbauer,[58] I. Howley,[71] Z. Hubacek,[7,15] V. Hynek,[7] I. Iashvili,[62] Y. Ilchenko,[72] R. Illingworth,[45] A. S. Ito,[45] S. Jabeen,[45,j] M. Jaffré,[13] A. Jayasinghe,[67] M. S. Jeong,[27] R. Jesik,[40] P. Jiang,[4,a] K. Johns,[42] E. Johnson,[57] M. Johnson,[45] A. Jonckheere,[45] P. Jonsson,[40] J. Joshi,[43] A. W. Jung,[45,k] A. Juste,[36] E. Kajfasz,[12] D. Karmanov,[33] I. Katsanos,[59] M. Kaur,[23] R. Kehoe,[72] S. Kermiche,[12] N. Khalatyan,[45] A. Khanov,[68] A. Kharchilava,[62] Y. N. Kharzheev,[31] I. Kiselevich,[32] J. M. Kohli,[23] A. V. Kozelov,[34] J. Kraus,[58] A. Kumar,[62] A. Kupco,[8] T. Kurča,[17] V. A. Kuzmin,[33] S. Lammers,[49] P. Lebrun,[17] H. S. Lee,[27] S. W. Lee,[52] W. M. Lee,[45,a] X. Lei,[42] J. Lellouch,[14] D. Li,[14] H. Li,[74] L. Li,[43] Q. Z. Li,[45] J. K. Lim,[27] D. Lincoln,[45] J. Linnemann,[57] V. V. Lipaev,[34,a] R. Lipton,[45] H. Liu,[72] Y. Liu,[4] A. Lobodenko,[35] M. Lokajicek,[8] R. Lopes de Sa,[45] R. Luna-Garcia,[28,l] A. L. Lyon,[45] A. K. A. Maciel,[1] R. Madar,[19] R. Magaña-Villalba,[28] S. Malik,[59] V. L. Malyshev,[31] J. Mansour,[20] J. Martínez-Ortega,[28] R. McCarthy,[64] C. L. McGivern,[41] M. M. Meijer,[29,30] A. Melnitchouk,[45] D. Menezes,[47] P. G. Mercadante,[3] M. Merkin,[33] A. Meyer,[18] J. Meyer,[20,m] F. Miconi,[16] N. K. Mondal,[25] M. Mulhearn,[74] E. Nagy,[12] M. Narain,[70] R. Nayyar,[42] H. A. Neal,[56,a] J. P. Negret,[5] P. Neustroev,[35] H. T. Nguyen,[74] T. Nunnemann,[22] J. Orduna,[70] N. Osman,[12] A. Pal,[71] N. Parashar,[50] V. Parihar,[70] S. K. Park,[27] R. Partridge,[70,n] N. Parua,[49] A. Patwa,[65,e] B. Penning,[40] M. Perfilov,[33] Y. Peters,[41] K. Petridis,[41] G. Petrillo,[63] P. Pétroff,[13] M.-A. Pleier,[65] V. M. Podstavkov,[45] A. V. Popov,[34] M. Prewitt,[73] D. Price,[41] N. Prokopenko,[34] J. Qian,[56] A. Quadt,[20] B. Quinn,[58] P. N. Ratoff,[39] I. Razumov,[34] I. Ripp-Baudot,[16] F. Rizatdinova,[68] M. Rominsky,[45] A. Ross,[39] C. Royon,[8] P. Rubinov,[45] R. Ruchti,[51] G. Sajot,[11] A. Sánchez-Hernández,[28] M. P. Sanders,[22] A. S. Santos,[1,o] G. Savage,[45] M. Savitskyi,[38] L. Sawyer,[54] T. Scanlon,[40] R. D. Schamberger,[64] Y. Scheglov,[35,a] H. Schellman,[69,48] M. Schott,[21] C. Schwanenberger,[41] R. Schwienhorst,[57] J. Sekaric,[53] H. Severini,[67] E. Shabalina,[20] V. Shary,[15] S. Shaw,[41] A. A. Shchukin,[34] O. Shkola,[38] V. Simak,[7,a] P. Skubic,[67] P. Slattery,[63] G. R. Snow,[59,a] J. Snow,[66] S. Snyder,[65] S. Söldner-Rembold,[41] L. Sonnenschein,[18] K. Soustruznik,[6] J. Stark,[11] N. Stefaniuk,[38] D. A. Stoyanova,[34] M. Strauss,[67] L. Suter,[41] P. Svoisky,[74] M. Titov,[15] V. V. Tokmenin,[31] Y.-T. Tsai,[63] D. Tsybychev,[64] B. Tuchming,[15] C. Tully,[61] L. Uvarov,[35] S. Uvarov,[35] S. Uzunyan,[47] R. Van Kooten,[49] W. M. van Leeuwen,[29] N. Varelas,[46] E. W. Varnes,[42] I. A. Vasilyev,[34] A. Y. Verkheev,[31] L. S. Vertogradov,[31] M. Verzocchi,[45] M. Vesterinen,[41] D. Vilanova,[15] P. Vokac,[7] H. D. Wahl,[44] C. Wang,[4] M. H. L. S. Wang,[45] J. Warchol,[51,a] G. Watts,[75] M. Wayne,[51] J. Weichert,[21] L. Welty-Rieger,[48] M. R. J. Williams,[49,p] G. W. Wilson,[53] M. Wobisch,[54] D. R. Wood,[55] T. R. Wyatt,[41] Y. Xie,[45] R. Yamada,[45] S. Yang,[4] T. Yasuda,[45] Y. A. Yatsunenko,[31,a] W. Ye,[64] Z. Ye,[45] H. Yin,[45] K. Yip,[65] S. W. Youn,[45] J. M. Yu,[56] J. Zennamo,[62] T. G. Zhao,[41] B. Zhou,[56] J. Zhu,[56] M. Zielinski,[63] D. Zieminska,[49] and L. Zivkovic[14,q]

(D0 Collaboration)

[1]*LAFEX, Centro Brasileiro de Pesquisas Físicas, Rio de Janeiro, RJ 22290, Brazil*
[2]*Universidade do Estado do Rio de Janeiro, Rio de Janeiro, RJ 20550, Brazil*
[3]*Universidade Federal do ABC, Santo André, SP 09210, Brazil*

072005-1

[4]*University of Science and Technology of China, Hefei 230026, People's Republic of China*
[5]*Universidad de los Andes, Bogotá, 111711, Colombia*
[6]*Charles University, Faculty of Mathematics and Physics, Center for Particle Physics,*
116 36 Prague 1, Czech Republic
[7]*Czech Technical University in Prague, 116 36 Prague 6, Czech Republic*
[8]*Institute of Physics, Academy of Sciences of the Czech Republic, 182 21 Prague, Czech Republic*
[9]*Universidad San Francisco de Quito, Quito 170157, Ecuador*
[10]*LPC, Université Blaise Pascal, CNRS/IN2P3, Clermont, F-63178 Aubière Cedex, France*
[11]*LPSC, Université Joseph Fourier Grenoble 1, CNRS/IN2P3,*
Institut National Polytechnique de Grenoble, F-38026 Grenoble Cedex, France
[12]*CPPM, Aix-Marseille Université, CNRS/IN2P3, F-13288 Marseille Cedex 09, France*
[13]*LAL, Université Paris-Sud, CNRS/IN2P3, Université Paris-Saclay, F-91898 Orsay Cedex, France*
[14]*LPNHE, Universités Paris VI and VII, CNRS/IN2P3, F-75005 Paris, France*
[15]*IRFU, CEA, Université Paris-Saclay, F-91191 Gif-Sur-Yvette, France*
[16]*IPHC, Université de Strasbourg, CNRS/IN2P3, F-67037 Strasbourg, France*
[17]*IPNL, Université Lyon 1, CNRS/IN2P3, F-69622 Villeurbanne Cedex, France and Université de Lyon,*
F-69361 Lyon CEDEX 07, France
[18]*III. Physikalisches Institut A, RWTH Aachen University, 52056 Aachen, Germany*
[19]*Physikalisches Institut, Universität Freiburg, 79085 Freiburg, Germany*
[20]*II. Physikalisches Institut, Georg-August-Universität Göttingen, 37073 Göttingen, Germany*
[21]*Institut für Physik, Universität Mainz, 55099 Mainz, Germany*
[22]*Ludwig-Maximilians-Universität München, 80539 München, Germany*
[23]*Panjab University, Chandigarh 160014, India*
[24]*Delhi University, Delhi-110 007, India*
[25]*Tata Institute of Fundamental Research, Mumbai-400 005, India*
[26]*University College Dublin, Dublin 4, Ireland*
[27]*Korea Detector Laboratory, Korea University, Seoul, 02841, Korea*
[28]*CINVESTAV, Mexico City 07360, Mexico*
[29]*Nikhef, Science Park, 1098 XG Amsterdam, The Netherlands*
[30]*Radboud University Nijmegen, 6525 AJ Nijmegen, The Netherlands*
[31]*Joint Institute for Nuclear Research, Dubna 141980, Russia*
[32]*Institute for Theoretical and Experimental Physics, Moscow 117259, Russia*
[33]*Moscow State University, Moscow 119991, Russia*
[34]*Institute for High Energy Physics, Protvino, Moscow region 142281, Russia*
[35]*Petersburg Nuclear Physics Institute, St. Petersburg 188300, Russia*
[36]*Institució Catalana de Recerca i Estudis Avançats (ICREA) and Institut de Física d'Altes Energies*
(IFAE), 08193 Bellaterra (Barcelona), Spain
[37]*Uppsala University, 751 05 Uppsala, Sweden*
[38]*Taras Shevchenko National University of Kyiv, Kiev, 01601, Ukraine*
[39]*Lancaster University, Lancaster LA1 4YB, United Kingdom*
[40]*Imperial College London, London SW7 2AZ, United Kingdom*
[41]*The University of Manchester, Manchester M13 9PL, United Kingdom*
[42]*University of Arizona, Tucson, Arizona 85721, USA*
[43]*University of California Riverside, Riverside, California 92521, USA*
[44]*Florida State University, Tallahassee, Florida 32306, USA*
[45]*Fermi National Accelerator Laboratory, Batavia, Illinois 60510, USA*
[46]*University of Illinois at Chicago, Chicago, Illinois 60607, USA*
[47]*Northern Illinois University, DeKalb, Illinois 60115, USA*
[48]*Northwestern University, Evanston, Illinois 60208, USA*
[49]*Indiana University, Bloomington, Indiana 47405, USA*
[50]*Purdue University Calumet, Hammond, Indiana 46323, USA*
[51]*University of Notre Dame, Notre Dame, Indiana 46556, USA*
[52]*Iowa State University, Ames, Iowa 50011, USA*
[53]*University of Kansas, Lawrence, Kansas 66045, USA*
[54]*Louisiana Tech University, Ruston, Louisiana 71272, USA*
[55]*Northeastern University, Boston, Massachusetts 02115, USA*
[56]*University of Michigan, Ann Arbor, Michigan 48109, USA*
[57]*Michigan State University, East Lansing, Michigan 48824, USA*
[58]*University of Mississippi, University, Mississippi 38677, USA*
[59]*University of Nebraska, Lincoln, Nebraska 68588, USA*

[60]Rutgers University, Piscataway, New Jersey 08855, USA

[61]Princeton University, Princeton, New Jersey 08544, USA

[62]State University of New York, Buffalo, New York 14260, USA

[63]University of Rochester, Rochester, New York 14627, USA

[64]State University of New York, Stony Brook, New York 11794, USA

[65]Brookhaven National Laboratory, Upton, New York 11973, USA

[66]Langston University, Langston, Oklahoma 73050, USA

[67]University of Oklahoma, Norman, Oklahoma 73019, USA

[68]Oklahoma State University, Stillwater, Oklahoma 74078, USA

[69]Oregon State University, Corvallis, Oregon 97331, USA

[70]Brown University, Providence, Rhode Island 02912, USA

[71]University of Texas, Arlington, Texas 76019, USA

[72]Southern Methodist University, Dallas, Texas 75275, USA

[73]Rice University, Houston, Texas 77005, USA

[74]University of Virginia, Charlottesville, Virginia 22904, USA

[75]University of Washington, Seattle, Washington 98195, USA

We present various properties of the production of the $X(3872)$ and $\psi(2S)$ states based on 10.4 fb^{-1} collected by the D0 experiment in Tevatron $p\bar{p}$ collisions at $\sqrt{s} = 1.96$ TeV. For both states, we measure the nonprompt fraction f_{NP} of the inclusive production rate due to decays of b-flavored hadrons. We find the f_{NP} values systematically below those obtained at the LHC. The f_{NP} fraction for $\psi(2S)$ increases with transverse momentum, whereas for the $X(3872)$ it is constant within large uncertainties, in agreement with the LHC results. The ratio of prompt to nonprompt $\psi(2S)$ production, $(1 - f_{NP})/f_{NP}$, decreases only slightly going from the Tevatron to the LHC, but for the $X(3872)$, this ratio decreases by a factor of about 3. We test the soft-pion signature of the $X(3872)$ modeled as a weakly bound charm-meson pair by studying the production of the $X(3872)$ as a function of the kinetic energy of the $X(3872)$ and the pion in the $X(3872)\pi$ center-of-mass frame. For a subsample consistent with prompt production, the results are incompatible with a strong enhancement in the production of the $X(3872)$ at the small kinetic energy of the $X(3872)$ and the π in the $X(3872)\pi$ center-of-mass frame expected for the $X +$ soft-pion production mechanism. For events consistent with being due to decays of b hadrons, there is no significant evidence for the soft-pion effect, but its presence at the level expected for the binding energy of 0.17 MeV and the momentum scale $\Lambda = M(\pi)$ is not ruled out.

[a]Deceased.

[b]Visitors from Augustana University, Sioux Falls, South Dakota 57197, USA.

[c]Visitors from Kiev Institute for Nuclear Research (KINR), Kyiv 03680, Ukraine.

[d]Visitors from The University of Liverpool, Liverpool L69 3BX, United Kingdom.

[e]Visitors from Office of Science, U.S. Department of Energy, Washington, D.C. 20585, USA.

[f]Visitors from Deutsches Elektronen-Synchrotron (DESY), Notkestrasse 85, Germany.

[g]Visitors from P. N. Lebedev Physical Institute of the Russian Academy of Sciences, 119991, Moscow, Russia.

[h]Visitors from CONACyT, M-03940 Mexico City, Mexico.

[i]Visitors from University College London, London WC1E 6BT, United Kingdom.

[j]Visitors from University of Maryland, College Park, Maryland 20742, USA.

[k]Visitors from Purdue University, West Lafayette, Indiana 47907, USA.

[l]Visitors from Centro de Investigacion en Computacion—IPN, CP 07738 Mexico City, Mexico.

[m]Visitors from Karlsruher Institut für Technologie (KIT)—Steinbuch Centre for Computing (SCC), D-76128 Karlsruhe, Germany.

[n]Visitors from SLAC, Menlo Park, California 94025, USA.

[o]Visitors from Universidade Estadual Paulista, São Paulo, SP 01140, Brazil.

[p]Visitors from European Orgnaization for Nuclear Research (CERN), CH-1211 Geneva, Switzerland.

[q]Visitors from Institute of Physics, Belgrade, Belgrade, Serbia.

I. INTRODUCTION

Fifteen years after the discovery of the state $X(3872)$ [1] (also named $\chi_{c1}(3872)$ [2]), its nature is still debated. Its proximity to the $D^0\bar{D}^{*0}$ threshold suggests a charm-meson molecule loosely bound by the pion exchange potential, first suggested by Tornqvist [3]. The molecular model also explains the isospin breaking decay to $J/\psi\rho$ that is not allowed for a pure charmonium state. However, the copious prompt production of the $X(3872)$ at hadron colliders has been used as an argument against a pure molecule interpretation [4]. With the binding energy less than 1 MeV, the average distance between the two components is a few femtometers. It has been argued that the production of such an extended object in the hadron collision environment is strongly disfavored and is better described by a compact charm-anticharm or diquark-antidiquark structure. Meng, Gao and Chao [5] proposed that the $X(3872)$ is a mixture of the conventional charmonium state $\chi_{c1}(2P)$ and a $D^0\bar{D}^{*0}$ molecule. In this picture, the short-distance production proceeds through the $\chi_{c1}(2P)$ component, while the $D^0\bar{D}^{*0}$ component is responsible for hadronic decays. An evaluation of the production cross section of the $X(3872)$ [6] through its $\chi_{c1}(2P)$ component gives a good description of the differential cross section for the prompt production of $X(3872)$ measured by CMS [7] and ATLAS [8].

Recently, Braaten *et al.* [9,10] have revised the calculation of the production of the $X(3872)$ under the purely molecular hypothesis by taking into account the formation of $D^*\bar{D}^*$ at short distances followed by the rescattering of the charm mesons onto $X\pi$. According to the authors, such a process should be easily observable at hadron colliders as an increased event rate at small values of the kinetic energy $T(X\pi)$ of the $X(3872)$ and the "soft" pion in the $X(3872)\pi$ center-of-mass frame and should provide a clean test of the molecular structure of the $X(3872)$.

In this article, we present production properties of the $X(3872)$ in Tevatron $p\bar{p}$ collisions at the energy $\sqrt{s} = 1.96$ TeV and compare them with those of the conventional charmonium state $\psi(2S)$. Section II describes relevant experimental details and the event selections. In Sec. III, we present the transverse momentum p_T and pseudorapidity η dependence of the fraction f_{NP} of the inclusive production rate due to nonprompt decays of b-flavored hadrons. In Sec. IV, we study the hadronic activity around the $X(3872)$ and $\psi(2S)$. We also test the soft-pion signature of the $X(3872)$ as a weakly bound charm-meson pair by studying the production of $X(3872)$ plus a comoving pion at small $T(X\pi)$. As a control process, we use the production of the charmonium state $\psi(2S)$, for which this production mechanism does not apply. We summarize the findings in Sec. V.

II. THE D0 DETECTOR, EVENT RECONSTRUCTION, AND SELECTION

The D0 detector has a central tracking system consisting of a silicon microstrip tracker and the central fiber tracker, both located within a 1.9 T superconducting solenoidal magnet [11,12]. A muon system, covering the pseudorapidity interval $|\eta| < 2$ [13], consists of a layer of tracking detectors and scintillation trigger counters in front of 1.8 T iron toroidal magnets, followed by two similar layers after the toroids [14]. Events used in this analysis are collected with both single-muon and dimuon triggers. Single-muon triggers require a coincidence of signals in trigger elements inside and outside the toroidal magnets. All dimuon triggers require at least one muon to have track segments after the toroid; muons in the forward region are always required to penetrate the toroid. The minimum muon transverse momentum is 1.5 GeV. No minimum p_T requirement is applied to the muon pair, but the effective threshold is approximately 4 GeV due to the requirement for muons to penetrate the toroids, and the average value for accepted events is 10 GeV.

We select two samples, referred to as 4-track and 5-track selections. To select 4-track candidates, we reconstruct $J/\psi \to \mu^+\mu^-$ decay candidates accompanied by two particles of opposite charge assumed to be pions, with transverse momentum p_T with respect to the beam axis greater than 0.5 GeV. We perform a kinematic fit under the hypothesis that the muons come from the J/ψ, and that the J/ψ and the two particles originate from the same space point. In the fit, the dimuon invariant mass is constrained to the world average value of the J/ψ meson mass [2]. The track parameters (p_T and position and direction in three dimensions) readjusted according to the fit are used in the calculation of the invariant mass $M(J/\psi\pi^+\pi^-)$ and the decay length vector $\vec{L}_{xy}$, which is the transverse projection of the vector directed from the primary vertex to the $J/\psi\pi^+\pi^-$ production vertex. The two-pion mass for each accepted $J/\psi\pi^+\pi^-$ candidate is required to be greater than 0.35 GeV (0.5 GeV) for $\psi(2S)$ ($X(3872)$) candidates. These conditions have a signal acceptance of more than 99% while reducing the combinatorial background. The transverse momentum of the $J/\psi\pi^+\pi^-$ system is required to be greater than 7 GeV. All tracks in a given event are considered, and all combinations of tracks satisfying the conditions stated are kept. The mass windows $3.62 < M(J/\psi\pi^+\pi^-) < 3.78$ GeV and $3.75 < M(J/\psi\pi^+\pi^-) < 4.0$ GeV are used for $\psi(2S)$ and $X(3872)$ selections, respectively. The rates of multiple entries within these ranges are less than 10%.

Fits to the $M(J/\psi\pi^+\pi^-)$ distribution for the 4-track selection are shown in Fig. 1. In the fits, the signal is modeled by a Gaussian function with a free mass and width. Background is described by a fourth-order Chebyshev polynomial. The fits yield 126891 ± 770 and 16423 ± 1031 events of $\psi(2S)$ and $X(3872)$, with mass parameters of 3684.88 ± 0.07 MeV and 3871.0 ± 0.2 MeV, and mass
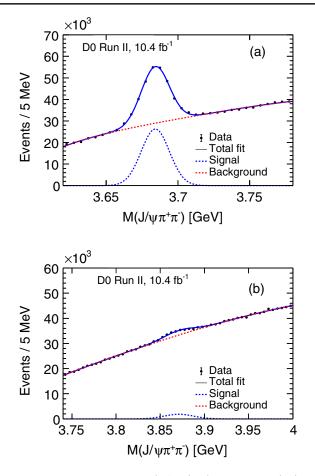
FIG. 1. The invariant mass $M(J/\psi\pi^+\pi^-)$ for (a) the $\psi(2S)$ and (b) the $X(3872)$ selection criteria for the 4-track selection.

FIG. 2. The invariant mass $M(J/\psi\pi^+\pi^-)$ for (a) the $\psi(2S)$ and (b) the $X(3872)$ selection criteria for the 5-track selection.

resolutions of 9.7 ± 0.1 MeV and 16.7 ± 0.9 MeV, respectively. These mass resolutions are used in all subsequent fits.

For the 5-track sample, we require the presence of an additional charged particle with $p_T > 0.5$ GeV, consistent with coming from the same vertex. We assume it to be a pion and set a mass limit $M(J/\psi\pi^+\pi^+\pi^-) < 4.8$ GeV. Charge-conjugate processes are implied throughout this article. To further reduce background, we allow up to two sets of three hadronic tracks per event, with an additional requirement that $M(J/\psi\pi^+\pi^-)$ be less than 4 GeV. With up to two accepted $J/\psi\pi^+\pi^-$ combinations per set, there are up to four accepted combinations per event. Because tracks are ordered by descending p_T, this procedure selects the highest-p_T tracks of each charge. Fits to the $M(J/\psi\pi^+\pi^-)$ distribution for the 5-track selection are shown in Fig. 2. The fits yield 75406 ± 1435 and 8192 ± 671 signal events of $\psi(2S)$ and $X(3872)$. The 5-track sample is used in the studies presented in Section IV.

III. PSEUDO-PROPER TIME DISTRIBUTIONS OF $\psi(2S)$ AND $X(3872)$

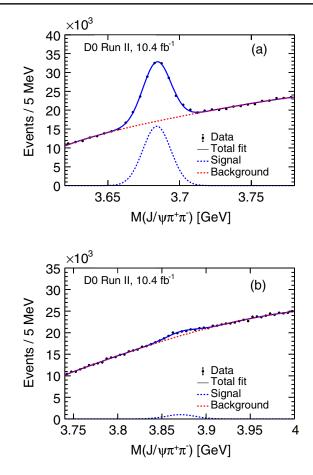In this section, we study the pseudo-proper time distributions for the charmonium states $\psi(2S)$ and $X(3872)$

using the 4-track sample. These states can originate from the primary $p\bar{p}$ interaction vertex (prompt production), or they can originate from a displaced secondary vertex corresponding to a beauty hadron decay (nonprompt production). The pseudo-proper time t_{pp} is calculated using the formula $t_{pp} = \vec{L}_{xy} \cdot \vec{p}_T m/(p_T^2 c)$, where $\vec{p}_T$ and m are the transverse momentum and mass of the charmonium state $\psi(2S)$ or $X(3872)$ expressed in natural units and c is the speed of light. We note that the true lifetimes of b hadrons decaying to $\psi(2S)$ or $X(3872)$ mesons are slightly different from the pseudo-proper time values obtained from the formula, because the boost factor of the charmonium is not exactly equal to the boost factor of the parent. Therefore, the nonprompt pseudoproper charmonium time distributions will have effective exponential lifetime values, which are close to but not equal to the lifetime for an admixture of B^0, B^-, B_s^0, B_c^- mesons, and b baryons.

To obtain the t_{pp} distributions, the numbers of events are extracted from fits for the $\psi(2S)$ and $X(3872)$ signals in mass distributions. This method removes combinatorial backgrounds and yields background-subtracted numbers of $\psi(2S)$ or $X(3872)$ signal events produced in each time interval. The bin width of the pseudo-proper time

distributions is chosen to increase exponentially to reflect the exponential shape of the lifetime distributions.

The fit function used to describe the $\psi(2S)$ mass distribution includes two terms: a single Gaussian used to model the signal and a third-order Chebyshev polynomial used to describe background. In the specific p_T and η intervals, the statistics in some t_{pp} bins may be insufficient for the fit to converge. In the case of a low number of background events, a second-order or a first-order Chebyshev polynomial is used. If the number of signal events is small, the signal Gaussian mass and width are fixed to the central values obtained in the fit to the distribution including all accepted events. Possible variations in the parameters appearing in this approach are estimated and are included in the systematic uncertainty.

The t_{pp} distribution for the $\psi(2S)$ sample is shown in Fig. 3. The numbers of events/0.0207 ps shown in Fig. 3 are obtained from fits to the mass distribution and corrected to the bin center to account for the steeply falling distribution.

The obtained t_{pp} distributions include prompt and non-prompt contributions. The prompt production is assumed to have a strictly zero lifetime, whereas the nonprompt component is assumed to be distributed exponentially starting from zero. These ideal signal distributions are smeared by the detector vertex resolution. The shape of the smearing function is expected to be the same for prompt and nonprompt production. Negative time values are possible due to the detector resolution of primary and secondary vertices. The pseudo-proper time distribution parametrization method is similar to that used in the
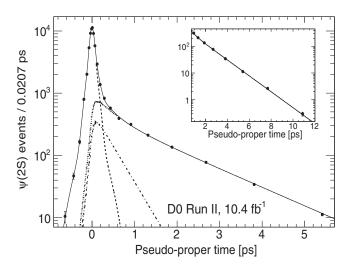

FIG. 3.   The number of events/0.0207 ps obtained using fits to the mass distributions for the $\psi(2S)$ sample in pseudo-proper time bins is shown. The tail of this distribution for the large-time region is given in the inset. The solid curve shows the result of the fit by the function described in the text. Also shown are contributions from the prompt component (dashed curve), the nonprompt component (dotted curve), and the short-lived component (dash-dotted curve) of the nonprompt production.

ATLAS analysis [8]. For the $\psi(2S)$ sample, the t_{pp} distributions are fitted using the χ^2 method with a model that includes prompt and nonprompt components:

$$F(t) = N[(1 - f_{NP})F_P(t) + f_{NP}F_{NP}(t)]. \qquad (1)$$

Here N is a free normalization factor, f_{NP} is a free parameter corresponding to the nonprompt contribution fraction, and $F_P(t)$ and $F_{NP}(t)$ are the shapes of the prompt and nonprompt components. The shape of the prompt component is modeled by a sum of three Gaussian functions with zero means and free normalizations and widths:

$$F_P(t) = g_1 G_1 + g_2 G_2 + g_3 G_3, \qquad (2)$$

where g_1, g_2, and g_3 are normalization parameters and G_1, G_2, and G_3 are Gaussian functions. The $\psi(2S)$ time distribution fit yields the three Gaussian widths $\sigma_1 = 0.0476 \pm 0.0016$ ps, $\sigma_2 = 0.1059 \pm 0.0047$ ps, and $\sigma_3 = 0.264 \pm 0.021$ ps, and the relative normalization factors $g_1 = 0.491 \pm 0.035$, $g_2 = 0.447 \pm 0.039$, and $g_3 = 0.062 \pm 0.013$.

The shape of the nonprompt function $F_{NP}(t)$ includes two terms, a short-lived (SL) component and a long-lived (LL) component:

$$F_{NP}(t) = (1 - f_{SL})F_{LL}(t) + f_{SL}F_{SL}(t). \qquad (3)$$

The f_{SL} is a free parameter in the fit. The long-lived and short-lived shape functions $F_{LL}(t)$ and $F_{SL}(t)$ are described by single exponential functions with slopes τ_{LL} and τ_{SL}, convolved with the resolution shape function that is the same as for the prompt component:

$$F_{LL}(t) = 1/\tau_{LL} \exp(-\tau_{LL}t) \otimes F_P(t), \qquad (4)$$

$$F_{SL}(t) = 1/\tau_{SL} \exp(-\tau_{SL}t) \otimes F_P(t). \qquad (5)$$

The long-lived component corresponds to charmonium production from B^0, B^+, B_s^0, and other b hadron decays, whereas the short-lived component is due to the B_c^+ decays. The production rate of the B_c^+ mesons in the $p\bar{p}$ collisions at 1.96 TeV is not well known. Theoretically, the ratio of B_c^+ meson production over all b hadrons is expected to be about 0.1%–0.2% [2]. However, the production ratio of B_c^+ to B^+ mesons has been measured by CDF [15], and an unexpectedly large value for this ratio between 0.9% and 1.9% was obtained; this ratio was calculated using theoretical predictions for the branching fraction $\mathcal{B}(B_c^+ \to J/\psi\mu^+\nu)$ to be in the range 1.15%–2.37% [15]. Assuming that the $\psi(2S)$ production rate in B_c^+ decays is enhanced by a factor of $\sim$20 compared with B^+, B^0, and B_s^0 decays, we expect a value of f_{SL} in the range of about 0.08–0.15. This factor can be estimated by taking into

account that the B_c^+ meson decays to charmonium states via the dominant "tree" diagram, whereas other B hadrons produce charmonium via the "color-suppressed" diagram. On the other hand, the short-lived component f_{SL} was measured by ATLAS [8] in pp collisions at the center-of-mass energy 8 TeV, and a value of a few percent was obtained for $\psi(2S)$, and one of $0.25 \pm 0.13 \pm 0.05$ for $X(3872)$. Because of the range of possible values, we include the short-lived term with a free normalization in the lifetime fit for the $\psi(2S)$ sample.

The t_{pp} distribution of the $\psi(2S)$ sample shown in Fig. 3 is well described by the function discussed above, where the exponential dependence is clearly seen in the large-time region. The fit quality is reasonably good, $\chi^2/\text{NDF} = 24.5/14$, corresponding to a p-value of 4%. This fit quality is adequate in view of the large range of numbers of events per bin and the simplicity of the pseudo-proper time fitting function. The fitted value of the short-lived component is $f_{SL} = 0.218 \pm 0.025$. If the short-lived component is neglected, a significantly larger value of $\chi^2 = 112$ is obtained. The parameters obtained from the fit shown in Fig. 3 are listed in Table I.

A similar method is used to obtain the pseudo-proper time distribution for the $X(3872)$ sample. The numbers of events/0.05 ps are shown in Fig. 4. Because the number of $X(3872)$ events is an order of magnitude smaller and the combinatorial background under the signal is slightly larger than for the $\psi(2S)$ sample, the number of t_{pp} bins for the mass fits is reduced from 24 to 12. The following assumptions are applied in the fit procedure: the vertex reconstruction resolution is the same for the $X(3872)$ and $\psi(2S)$ states, and the short-lived and long-lived component lifetimes and relative rates are fixed for the $X(3872)$ to the values obtained from the $\psi(2S)$ fit. These assumptions are based on similarity in production kinematics and an only 5% difference in the masses of these states. The relative short-lived and long-lived rates are expected to be similar, if the ratio of inclusive branching fractions from the B_c^+ and other B hadrons is similar for the $X(3872)$ and $\psi(2S)$ states. The uncertainties of these assumptions are estimated and included in systematics. These systematic uncertainties are significantly smaller than the statistical uncertainties, because the f_{NP} values for $X(3872)$ are small and the statistical uncertainties are large. Therefore, in the $X(3872)$ t_{pp} fit procedure, all parameters are fixed to the
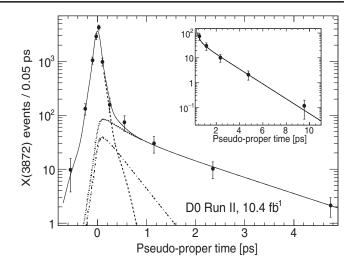

FIG. 4. The number of events/0.05 ps obtained using fits to the mass distributions for the $X(3872)$ sample in pseudo-proper time bins is shown. The tail of this distribution for the large-time region is given in the inset. The curve shows the result of the fit to the function described in the text. Also shown are contributions from the prompt component (dashed curve), the nonprompt component (dotted curve), and the short-lived component (dash-dotted curve) of the nonprompt production.

values obtained in the $\psi(2S)$ pseudo-proper time fit, except the f_{NP} parameter. The prompt signal Gaussian widths are scaled by the mass ratio $M(X(3872))/M(\psi(2S))$ to correct for the difference in the boost factors of the $X(3872)$ sample relative to the $\psi(2S)$ sample, which results in a different time resolution for the same spatial resolution. We obtain $f_{NP} = 0.139 \pm 0.025$ from the fit with $\chi^2/\text{NDF} = 8.1/10$.

The systematic uncertainties on f_{NP} estimated for the full p_T region are listed in Table II. They include the uncertainty due to (1) the muon reconstruction and identification efficiencies, (2) variation of the pion reconstruction efficiency in the low- and high-t_{pp} regions, (3) different p_T distribution shapes for the prompt and

TABLE I. The parameters obtained from the $\psi(2S)$ sample fit shown in Fig. 3.

Parameter	Fitted values, $\psi(2S)$
f_{NP}	0.328 ± 0.006 ps
f_{SL}	0.218 ± 0.025 ps
τ_{LL}	1.456 ± 0.026 ps
τ_{SL}	0.38 ± 0.06 ps

TABLE II. The systematic uncertainties in f_{NP} (in percent) of the $\psi(2S)$ and $X(3872)$ states.

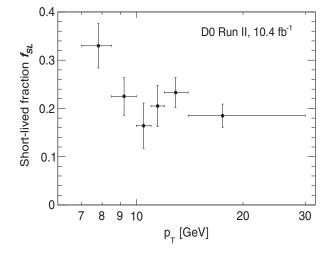| Parameter	$\psi(2S)$	$X(3872)$
Muon reconstruction/ID efficiency	± 0.1	± 0.1
Pion reconstruction efficiency	$^{+0.7}_{-0.3}$	$^{+0.4}_{-0.2}$
p_T distributions	± 0.3	± 0.2
Mass fit model	$^{+0.5}_{-1.0}$	$^{+0.5}_{-0.7}$
Resolution function	± 0.1	± 0.1
Short-lived (SL) component shape	± 0.3	$^{+0.3}_{-0.2}$
Long-lived (LL) component shape	± 0.2	$^{+0.3}_{-0.2}$
Ratio of LL and SL components	$^{+0.1}_{-0.5}$	$^{+0.5}_{-0.4}$
Sum	$^{+1.0}_{-1.3}$	± 0.9

FIG. 5. The short-lived component fraction f_{SL} as a function of p_T for the $\psi(2S)$ states. Only statistical uncertainties are shown.

TABLE III. The values of nonprompt fractions f_{NP} for the $\psi(2S)$ and $X(3872)$ states in p_T and η intervals with the statistical and systematic uncertainties are given.

	$\psi(2S)$		$X(3872)$
All	$0.328 \pm 0.006^{+0.010}_{-0.013}$		$0.139 \pm 0.025 \pm 0.009$
p_T, GeV		p_T, GeV	
7–8.5	$0.244 \pm 0.008^{+0.010}_{-0.021}$	7–10	$0.128 \pm 0.046^{+0.009}_{-0.008}$
8.5–10	$0.275 \pm 0.007^{+0.013}_{-0.016}$		
10–11	$0.304 \pm 0.009^{+0.011}_{-0.020}$	10–12	$0.156 \pm 0.038^{+0.016}_{-0.014}$
11–12	$0.312 \pm 0.010^{+0.010}_{-0.017}$		
12–14	$0.365 \pm 0.008^{+0.013}_{-0.021}$	12–30	$0.121 \pm 0.047^{+0.010}_{-0.006}$
14–30	$0.427 \pm 0.007^{+0.013}_{-0.024}$		

	$\psi(2S)$	$X(3872)$
$\|\eta\| < 1$	$0.344 \pm 0.007^{+0.014}_{-0.020}$	$0.164 \pm 0.035^{+0.009}_{-0.016}$
$1 < \|\eta\| < 2$	$0.303 \pm 0.008^{+0.017}_{-0.020}$	$0.116 \pm 0.032^{+0.009}_{-0.010}$

nonprompt events, (4) variation of the mass fit model parameters, (5) variation of the time resolution function, (6) variation of the short-lived function shape, (7) variation of the long-lived function shape, and (8) production ratio of the short-lived and long-lived components.

For the full p_T range studied, we obtain $f_{NP} = 0.328 \pm 0.006^{+0.010}_{-0.013}$ for the $\psi(2S)$ meson sample and $f_{NP} = 0.139 \pm 0.025 \pm 0.009$ for the $X(3872)$ meson sample, where the first uncertainty is statistical and the second is systematic.

The large sample sizes allow us to study the t_{pp} distributions in several p_T intervals. We choose six p_T intervals for the $\psi(2S)$ and three for the $X(3872)$. In addition, the fit procedure is performed by dividing the full data samples into two $\psi(2S)$ and $X(3872)$ pseudorapidity intervals: $|\eta| < 1$ and $1 < |\eta| < 2$. The method used to obtain parameters is the same as for the full data sample. For a given p_T or η interval, we first fit the $\psi(2S)$ t_{pp} distribution and obtain the free parameters. Then, these parameters are fixed in the fit of the $X(3872)$ t_{pp} distribution. For both mesons, the fraction f_{NP} of the nonprompt component is allowed to vary in each p_T or η interval. Figure 5 shows the p_T dependence of f_{SL} for the $\psi(2S)$; the values of this parameter are larger than the values of a few percent obtained by the ATLAS Collaboration [8].

For all measured f_{NP} values, the systematic uncertainties are calculated applying the same procedure and the same variation intervals as for the whole data sample. The values of nonprompt fractions for the $\psi(2S)$ and $X(3872)$ states in different p_T or η intervals with the statistical and systematic uncertainties are given in Table III. Figure 6 shows f_{NP} as a function of p_T for the $\psi(2S)$, compared with the ATLAS [8] measurement at 8 TeV, the CMS [16] measurement at 7 TeV, and the CDF [17] measurement at 1.96 TeV. Figure 7 shows similar distributions for the $X(3872)$ obtained in this analysis, together with the ATLAS [8]

and CMS [7] measurements. The D0 measurements of f_{NP} are systematically below the ATLAS [8] and CMS [7] points obtained at higher c.m. energies, although the LHC measurements are restricted to more central pseudorapidity regions. The small differences between the CDF and D0 $\psi(2S)$ measurements can be ascribed to differences in pseudorapidity acceptance. However, the general tendencies are very similar: the f_{NP} values increase with p_T in the case of $\psi(2S)$ state production, whereas the f_{NP} values for $X(3872)$ are independent of p_T within large uncertainties.
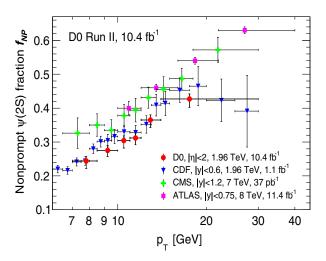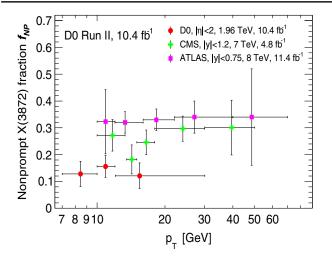

FIG. 6. The nonprompt component f_{NP} for the $\psi(2S)$ states as a function of p_T. Red circles correspond to this analysis, magenta boxes to the ATLAS [8] measurement, green crosses to the CMS [16] measurement, and blue triangles to CDF [17]. The uncertainties shown are total uncertainties, except for the CDF points, for which only the statistical uncertainties are displayed. The D0 and ATLAS analyses are performed using $\psi(2S) \to J/\psi\pi^+\pi^-$ decay channel, whereas the CMS and CDF data are obtained through the $\psi(2S) \to \mu^+\mu^-$ decay.

FIG. 7. The nonprompt component f_{NP} for the $X(3872)$ states as a function of p_T. Red circles correspond to this analysis, magenta boxes to the ATLAS [8] measurement and green crosses to the CMS [7] measurement. The uncertainties shown are total uncertainties.

We summarize the measurements of this section as follows:

(1) The nonprompt fractions for $\psi(2S)$ increase as a function of p_T, whereas those for $X(3872)$ are consistent with being independent of p_T. These trends are similar to those seen at the LHC. The Tevatron values tend to be somewhat smaller than those measured by ATLAS and CMS.

(2) The ratio of prompt to nonprompt $\psi(2S)$ production, $R_{p/np} = (1 - f_{NP})/f_{NP}$, increases only slightly going from the LHC to the Tevatron. As can be seen in Fig. 6, the f_{NP} values in the 9–10 GeV range are 0.35 ± 0.03 for LHC data and 0.30 ± 0.02 for Tevatron data, resulting in increase in $R_{p/np}$ of $(7-47)\%$ (68.3% confidence interval). At low p_T, the CMS data points have large statistical uncertainties, but the Tevatron data can be compared to the LHCb measurement of $\psi(2S)$ f_{NP} values [18] at 7 TeV for $2.0 < y < 2.5$ and $6 < p_T < 14$ GeV. The LHCb $R_{p/np}$ values are about $(25-30)\%$ smaller than those from the Tevatron, after adjustment for the variation with pseudorapidity. The LHCb data indicate a reduction of f_{NP} by 0.02–0.03 for each reduction in rapidity by one unit.

(3) The ATLAS value of $f_{NP} = 0.328 \pm 0.026$ for the $X(3872)$ differs from the D0 value of $f_{NP} = 0.139 \pm 0.027$ by 5.0σ, taking into account both statistical and systematic uncertainties and assuming a uniform p_T distribution. This gives an increase in the $R_{p/np}$ ratio by a factor of ~ 3 (the range 2.4–4.0 for the 68.3% confidence interval) going from the LHC to the Tevatron. It has to be noted that this difference may be partially compensated by the larger rapidity interval covered by D0. This increase

of the $R_{p/np}$ value indicates that the prompt production of the exotic state $X(3872)$ relative to the b hadron production is strongly suppressed at the LHC in comparison with the Tevatron conditions. This suppression is possibly due to more particles produced in the primary collision at LHC that increase the probability to disassociate the nearly unbound and possibly spatially extended $X(3872)$ [19,20].

IV. HADRONIC ACTIVITY AROUND THE ψ(2S) AND X(3872) STATES

In this section, we study the association of the $\psi(2S)$ or $X(3872)$ states with another particle assumed to be a pion using the 5-track sample. We study the dependence of the production of these two states on the surrounding hadronic activity. We also test the soft-pion signature of the $X(3872)$ as a weakly bound charm-meson pair by studying the production of $X(3872)$ at small kinetic energy of the $X(3872)$ and the π in the $X(3872)\pi$ center-of-mass frame.

The data are separated into a "prompt" sample, defined by the conditions $L_{xy} < 0.025$ cm and $L_{xy}/\sigma(L_{xy}) < 3$, and a "nonprompt" sample defined by $L_{xy} > 0.025$ cm and $L_{xy}/\sigma(L_{xy}) > 3$, where L_{xy} is the decay length of the $J/\psi\pi^+\pi^-$ system in the transverse plane.

In these studies, the uncertainties in the results are dominated by the statistical uncertainties in the fitted $X(3872)$ yields. In the limited mass range around the $\psi(2S)$ or $X(3872)$, the background is smooth and monotonic, and is well described by low-order Chebyshev polynomials. Depending on the size of a given subsample, the polynomial order is set to 2 or 3. In all cases, the difference between the yields for the two background choices is less than 30% of the statistical uncertainty. The small systematic uncertainties are ignored.

A. ψ(2S) and X(3872) isolation

The LHCb Collaboration has studied [20] the dependence of production cross sections of the $X(3872)$ and $\psi(2S)$ on the hadronic activity in an event, which is approximated using a measure of the charged particle multiplicity. The authors found the ratio of the cross sections for promptly produced particles, $\sigma(X(3872))/\sigma(\psi(2S))$, to decrease with increasing multiplicity and observed that this behavior is consistent with the interpretation of the $X(3872)$ as a weakly bound state, such as a $D^0\bar{D}^{*0}$ hadronic molecule. In this scenario, interactions with comoving hadrons produced in the collision disassociate the large, weakly bound $X(3872)$ state more than the relatively compact conventional charmonium state $\psi(2S)$.

In this study of the production of charmonium-like states, we introduce *isolation* as an observable quantifying the hadronic activity in a restricted cone in the $\phi - \eta$ space around the candidate, $\Delta R = \sqrt{\Delta\phi^2 + \Delta\eta^2}$. We define the isolation as a ratio of the candidate's momentum to the
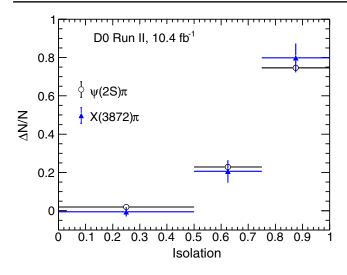
FIG. 8.   Normalized yields of the $\psi(2S)\pi$ (black open circles) and the $X(3872)\pi$ (blue triangles) as functions of isolation for the prompt sample.

scalar sum of the momenta of all charged particles pointing to the primary vertex produced in a cone of $\Delta R = 1$ around the candidate and the candidate itself. Distributions of isolation for prompt $\psi(2S)\pi$ and $X(3872)\pi$ normalized to unity are shown in Fig. 8, and the ratio of the un-normalized distributions is shown in Fig. 9. The shapes of the two isolation distributions are similar. The difference between the χ^2 values obtained for fits to the ratio as a function of isolation assuming a free slope and zero slope corresponds to 1.2σ. This gives modest support for the hypothesis that increased hadronic activity near $X(3872)$ depresses its production.

B. Search for the soft-pion effect

Recent theoretical work [9,10] predicts a sizable contribution to the production of the $X(3872)$, both directly in

FIG. 9.   The ratio of the unnormalized $X(3872)$ and $\psi(2S)$ yields as a function of isolation for the prompt sample.

the hadronic beam collisions and in b hadron decays, from the formation of the $X(3872)$ in association with a comoving pion. According to the authors, the $X(3872)$, assumed to be a $D\bar{D}^*$ molecule, is produced by the creation of $D\bar{D}^*$ at short distances. But it can also be produced by the creation of $D^*\bar{D}^*$ at short distances, followed by a rescattering of the charm-meson pair into a $X(3872)\pi$ pair by exchanging a D meson. The cross section from this mechanism would have a narrow peak in the $X(3872)\pi$ invariant mass distribution near the $D^*\bar{D}^*$ threshold from a triangle singularity that occurs when the three particles participating in a rescattering are all near the mass shell.

A convenient variable to quantify this effect is the kinetic energy $T(X\pi)$ of the $X(3872)$ and the π in the $X(3872)\pi$ center-of-mass frame. The authors define the peak region to be $0 \leq T(X\pi) \leq 2\delta_1$, where $\delta_1 = M(D^{*+}) - M(D^0) - M(\pi^+) = 5.9$ MeV. The effect is sensitive to the $D\bar{D}^*$ binding energy, whose current estimated value is (-0.01 ± 0.18) MeV. The peak height is expected to decrease with increasing binding energy. It also depends on the value of the momentum scale Λ, expected to be of the order of $M(\pi^+)$. For the conservative choice of a binding energy of 0.17 MeV, the yield in the peak region is predicted to be smaller than the yield without a soft pion by a factor $\sim 0.14(M(\pi^+)/\Lambda)^2$. For $\Lambda = M(\pi^+)$, this ratio is equal to 0.14. We search for this effect separately in the "prompt" and "nonprompt" samples.

1. Prompt production

As a benchmark, we use the $\psi(2S)$, for which no soft-pion effect is expected. We select combinations $J/\psi\pi^+\pi^+\pi^-$ that have a $J/\psi\pi^+\pi^-$ combination in the mass range $3.62 < M(J/\psi\pi^+\pi^-) < 3.74$ GeV. The total number of entries is 310 636, and the $\psi(2S)$ signal has 48711 ± 511 events. The mass distributions and fits are shown in Fig. 10. After the $T(\psi(2S)\pi) < 11.8$ MeV cut, the number of entries is 368, and the signal yield is 44 ± 14 events. The cut $T(\psi(2S)\pi) < 11.8$ MeV keeps a fraction 0.0009 ± 0.0003 of the signal, in agreement with the measured reduction of the combinatorial background by a factor of 0.0012. As expected, there is no evidence for a soft-pion effect for $\psi(2S)$.

Then, we select $J/\psi\pi^+\pi^+\pi^-$ combinations that have a $J/\psi\pi^+\pi^-$ combination in the mass range $3.75 < M(J/\psi\pi^+\pi^-) < 4.0$ GeV, that includes the $X(3872)$. The total number of selected entries is 749 179, and the $X(3872)$ signal yield is 6157 ± 599 events. The mass distributions and fits are shown in Fig. 11. The signal consists of a $X(3872)$ meson produced together with a charged particle. It includes possible pairs of a $X(3872)$ meson and an associated soft pion from the triangle singularity. The background is due to random combinations of a J/ψ meson and three charged particles. The cut $T(X\pi) < 11.8$ MeV should remove the bulk of random $X(3872)$-pion combinations while keeping the events due
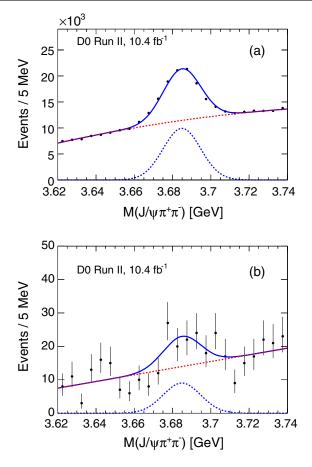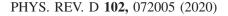
FIG. 10. $M(J/\psi\pi^+\pi^-)$ distribution and fits for the $\psi(2S)$ signal for the prompt subsample for (a) all selected events and (b) events passing the $T(\psi(2S)\pi) < 11.8$ MeV cut.

FIG. 11. $M(J/\psi\pi^+\pi^-)$ distribution and fits for the $X(3872)$ signal for the prompt subsample for (a) all selected events and (b) events passing the $T(X\pi) < 11.8$ MeV cut.

to the triangle singularity. For this subsample of 730 events, the fitted signal yield is 18 ± 16 events. Thus, the cut $T(X\pi) < 11.8$ MeV keeps a fraction 0.003 ± 0.003 of the signal, consistent with the background reduction by a factor of 0.00097 ± 0.00004. In the absence of the soft-pion process, the expected yield at small $T(X\pi)$ is $N = 6157 \times 0.00097 = 6$ events. With the measured yield of 18 ± 16 events, the net excess is 12 ± 16 events. The 90% C.L. upper limit is 43 events, which is less than 0.007 of the total number of accepted events.

To compare this result with the expected number of accepted soft-pion events, we make a rough estimate of the kinematic acceptance for events above and below the 11.8 MeV cutoff. The main factor is the loss of pions produced with $p_T < 0.5$ GeV that strongly depends on $T(X\pi)$, given the p_T distribution of the $X(3872)$.

The transverse momentum distributions of pions in the two subsamples are shown in Fig. 12. Above 0.5 GeV, the distributions fall exponentially. Below the 0.5 GeV threshold, the spectrum must rise from the minimum kinematically allowed value to a peak followed by the exponential falloff. For events with $T(X\pi) > 11.8$ MeV, we fit the distribution to the function $N p_T \exp(-p_T/p_{T0})$ and define
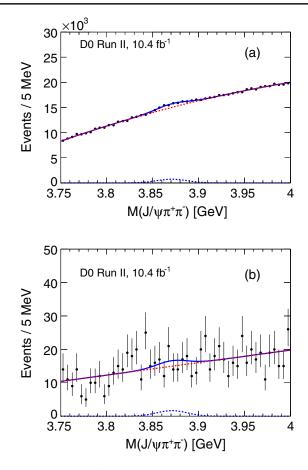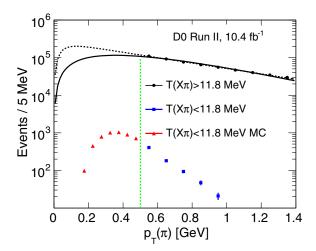

FIG. 12. Transverse momentum distribution of pion candidates for events above and below the $T(X\pi) = 11.8$ MeV cutoff for prompt events in the mass range $3.75 < M(J/\psi\pi^+\pi^-) < 4$ GeV. The former is compared to two fits discussed in the text. Extrapolation of the latter below threshold follows the method described in the text.

the acceptance A as the ratio of the integral from 0.5 GeV to infinity to the integral from zero to infinity. The result is 0.6. With alternate functions, the acceptance values vary from 0.3 to 0.9. Figure 12 shows two fits with similar behavior above threshold but different below threshold, the default function and the function $N(1 - \exp(-p_T/p_{T1})) \exp(-p_T/p_{T2})$.

For events with $T(X\pi) < 11.8$ MeV, the p_T distribution of the accompanying pion is closely related to the p_T of the $X(3872)$. To determine the pion acceptance, we employ a simplified MC model, starting with the differential cross section as a function of $T(X\pi) < 11.8$ MeV given in Ref. [9]. For a $X(3872)$ with a given $p_T(X)$, the X and pion are distributed isotropically in the $X\pi$ rest frame. The transverse momentum of the pion $p_T(\pi)$ in the laboratory frame is determined by transforming to the $X(3872)$ rest frame, using the chosen $p_T(X)$ and a rapidity $y(X)$ chosen from a uniform distribution $|y| < 2$, and then transforming to the laboratory frame. The pion acceptance as a function of $p_T(X)$, $A(p_T(X))$, is then convolved with the fitted $X(3872)$ yield $dN/dp_T(X)$ as a function of $p_T(X)$ to determine the overall acceptance for pions.

Our observed dN/dp_T distribution for the $X(3872)$ is found by dividing the mass distribution for $J/\psi\pi^+\pi^-$ in Fig. 11(a) for the 5-track sample into seven p_T bins each 2 GeV wide, between 7 and 21 GeV, and fitting for the yield of the $X(3872)$ for each bin. This produces a background-subtracted sample; however, it has relatively large statistical
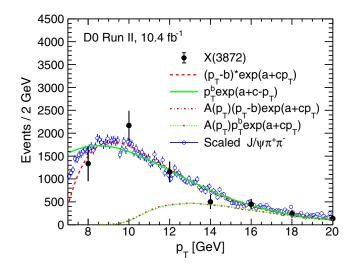

FIG. 13. The transverse momentum distribution for the background-subtracted mass-fitted $X(3872)$ (filled circles), and two fits representing the high and low ranges of the acceptance for the accompanying pion. The dashed curves represent $A(p_T)dN/dp_T(X(3872))$. The overall acceptance for the accompanying pion is the ratio of the areas below $AdN/p_T(X)$ curves and the corresponding $dN/dp_T(X)$ fits. For comparison, the scaled p_T distribution of the inclusive $J/\psi\pi\pi$ for $3.85 < M(J/\psi\pi^+\pi^-) < 3.9$ GeV (open blue circles) is overlaid, illustrating their similarity in shape.

uncertainties. These seven dN/dp_T yield points for the $X(3872)$ are plotted in Fig. 13. The higher statistics and finer-binned yield for inclusive $J/\psi\pi^+\pi^-$ events over the mass range 3850–3900 MeV of Fig. 11(a) as a function of p_T is used to check the shape of the p_T distribution of the $X(3872)$. After scaling to equal areas, $dN/dp_T(J/\psi\pi^+\pi^-)$ shows a good agreement within statistical uncertainties with the $X(3872)$ spectrum, thus indicating a comparable behavior of the $X(3872)$ signal and background.

Fits of the background-subtracted yields using the functions $p_T^b\exp(a + cp_T)$ and $(p_T - b)\exp(a + cp_T)$ are shown in Fig. 13, along with the products $A(p_T)dN/dp_T$, which allow the calculation of the acceptance for $p_T(\pi) > 0.5$ GeV for events with $p_T(X) > 7$ GeV. We find the acceptances $A = 0.278 \pm 0.031$ and 0.296 ± 0.036 for the two functions, respectively, where the uncertainties are due to the statistical uncertainty in the determination of the $dN/dp_T(X)$ distribution. Additional functions were used to fit $dN/dp_T(X)$. The aforementioned functions yield the lowest and highest pion acceptances obtained from the different forms. Their difference is considered as the systematic uncertainty associated with the choice of parametrization. We average the two results to obtain $A = 0.29 \pm 0.03(\text{stat}) \pm 0.02(\text{syst})$.

For the prompt case, this leads to the expected number of produced $X(3872)$ events at $N = 18/0.29 + 6139/0.6 \approx 10000$ with an uncertainty of about $\pm 50\%$. With $N = N_1 + N_0$, where N_1 is the number of events with a soft pion, and the relation $N_1 = 0.14N_0$, $N \approx 10000 \times 0.14/1.14 \approx 1300$ events would be produced through the soft-pion process with an uncertainty of about 650 events, and between 245 and 730 would be accepted. That is much larger than the observed 12 ± 16 events. We conclude that there is no evidence for the soft-pion effect in the prompt sample.

2. Nonprompt production

The kinematics of the prompt and nonprompt samples are sufficiently similar to use the acceptance derived for the prompt case for both samples. Calculations analogous to those for the prompt case give the following results for the nonprompt sample. For the $\psi(2S)$, the kinetic energy cut keeps a fraction of 0.004 ± 0.001 of the signal, in agreement with the reduction by a factor of 0.003 of the total number of entries.

For the $X(3872)$, the signal yields before and after the cut are 703 ± 25 and 27 ± 12, respectively. The cut accepts a fraction 0.04 ± 0.02 of the signal. The corresponding reduction in the total number of events in the distribution is by a factor of 0.0029 ± 0.0001. For a random pairing of the $X(3872)$ with a pion, the expected yield at small $T(X\pi)$ is $N = 703 \times 0.0029 = 2$ events, leading to a net excess of 25 ± 12 events. The statistical significance of the excess, based on the χ^2 difference between the fit with a free signal yield and the fixed value of $N = 2$ expected for the
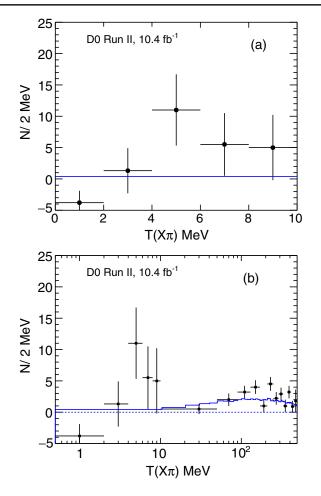
FIG. 14. The fitted $X(3872)$ signal yield as a function of $T(X\pi)$ for nonprompt events with (a) the soft-pion production region and (b) extended range. The first five points in (b) are the same as those in (a). The blue line shows the distribution of the $T(X\pi)$ for all nonprompt $X(3872)$ candidates scaled down to the total $X(3872)$ yield.

"random pairing only" case, is 2σ. Correcting for soft-pion acceptance, the number of produced nonprompt $X(3872)$ before the kinematic cut is in the range 800–2000. Assuming the ratio of 0.14 between the cross section for production with a soft pion to the cross section for production without a soft pion [9], we estimate the expected number of produced soft-pion events to be in the range 100–300. With the acceptance of 0.29 ± 0.04, the expected number of accepted soft-pion events is between 30 and 90. The measured excess yield of 25 ± 12 events is in agreement with this expectation; however, the fact that our yield agrees within 2σ with the null hypothesis of no soft-pion events prevents drawing a definite conclusion.

For further details on the distribution of the nonprompt signal versus $T(X\pi)$, we fit the $X(3872)$ mass distributions into 2 MeV bins of $T(X\pi)$ from 0 to 10 MeV and into 40 MeV bins from 10 to 490 MeV. The resulting distribution of events/2 MeV is shown in Fig. 14. Above ~ 10 MeV, the observed spectrum is consistent with the

pairing of a $X(3872)$ with a random particle. It is similar to the $T(X\pi)$ distribution of all nonprompt $X(3872)$ candidates. At lower $T(X\pi)$, there is a small excess, with a significance of 2σ, above the random pairing, at the level consistent with the predictions of Ref. [9]. We again conclude that there is no significant evidence for the soft-pion effect, but its presence at the level expected for the binding energy of 0.17 MeV and the momentum scale $\Lambda = M(\pi)$ is not ruled out.

V. SUMMARY AND CONCLUSIONS

We have presented various properties of the production of the $\psi(2S)$ and $X(3872)$ in Tevatron $p\bar{p}$ collisions. For both states, we have measured the fraction f_{NP} of the inclusive production rate due to decays of b-flavored hadrons as a function of the transverse momentum p_T. Our nonprompt fractions for $\psi(2S)$ increase as a function of p_T, whereas those for $X(3872)$ are consistent with being independent of p_T. These trends are similar to those seen at the LHC. The Tevatron values tend to be somewhat smaller than those measured by ATLAS and CMS, but this difference can at least partially be accounted for by the larger rapidity interval covered by D0. The ratio of prompt to nonprompt $\psi(2S)$ production, $(1 - f_{NP})/f_{NP}$, decreases only slightly going from the Tevatron to the LHC, but in comparing the 8 TeV ATLAS data to the 1.96 TeV D0 data for the $X(3872)$ production, this ratio decreases by a factor of approximately 3. This indicates that the prompt production of the exotic state $X(3872)$ is suppressed at the LHC, possibly due to the production of more particles in the primary collision that increases the probability to disassociate the nearly unbound and possibly more spatially extended $X(3872)$ state.

We have tested the soft-pion signature of the $X(3872)$ modeled as a weakly bound charm-meson pair by studying the production of the $X(3872)$ as a function of the kinetic energy of the $X(3872)$ and the pion in the $X\pi$ center-of-mass frame. For a subsample consistent with prompt production, the results are incompatible with a strong enhancement in the production of the $X(3872)$ at small $T(X\pi)$ expected for the $X +$ soft-pion production mechanism. For events consistent with being due to decays of b hadrons, there is no significant evidence for the soft-pion effect, but its presence at the level expected for the binding energy of 0.17 MeV and the momentum scale $\Lambda = M(\pi)$ is not ruled out.

[1] S.-K. Choi *et al.* (Belle Collaboration), Observation of a Narrow Charmonium-Like State in Exclusive $B^{\pm} \to K^{+-}\pi^{+}\pi^{-}J/\psi$ Decays, Phys. Rev. Lett. **91,** 262001 (2003).

[2] P. A. Zyla *et al.* (Particle Data Group), The review of particle physics 2020, Prog. Theor. Exp. Phys. **2020,** 083C01 (2020).

[3] N. A. Törnqvist, Isospin breaking of the narrow charmonium state of Belle at 3872 MeV as a deuson, Phys. Lett. B **590,** 209 (2004).

[4] C. Bignamini, B. Grinstein, F. Piccinini, A. D. Polosa, and C. Sabelli, Is the $X(3872)$ Production Cross Section at $\sqrt{s} = 1.96$ TeV Compatible with a Hadron Molecule Interpretation? Phys. Rev. Lett. **103,** 162001 (2009).

[5] C. Meng, Y.-J. Gao, and K.-T. Chao, $B \to \chi_{c1}(1P, 2P)K$ decays in QCD factorization and $X(3872)$, Phys. Rev. D **87,** 074035 (2013).

[6] C. Meng, H. Han, and K.-T. Chao, $X(3872)$ and its production at hadron colliders, Phys. Rev. D **96,** 074014 (2017).

[7] S. Chatrchyan *et al.* (CMS Collaboration), Measurement of the $X(3872)$ production cross section via decays to $J/\psi\pi^{+}\pi^{-}$ in pp collisions at $\sqrt{s} = 7$ TeV, J. High Energy Phys. 04 (2013) 154.

[8] M. Aaboud *et al.* (ATLAS Collaboration), Measurements of $\psi(2S)$ and $X(3872) \to J/\psi\pi^{+}\pi^{-}$ production in pp collisions at $\sqrt{s} = 8$ TeV with the ATLAS detector, J. High Energy Phys. 01 (2017) 117.

[9] E. Braaten, L.-P. He, and K. Ingles, Production of $X(3872)$ accompanied by a soft pion at hadron colliders, Phys. Rev. D **100,** 094006 (2019).

[10] E. Braaten, L.-P. He, and K. Ingles, Production of $X(3872)$ accompanied by a pion in B meson decay, Phys. Rev. D **100,** 074028 (2019).

[11] V. M. Abazov *et al.* (D0 Collaboration), The upgraded D0 detector, Nucl. Instrum. Methods Phys. Res., Sect. A **565,** 463 (2006).

[12] R. Angstadt *et al.*, The layer 0 inner silicon detector of the D0 experiment, Nucl. Instrum. Methods Phys. Res., Sect. A **622,** 298 (2010).

[13] $\eta = -\ln[\tan(\theta/2)]$ is the pseudorapidity, and θ is the polar angle between the track momentum and the proton beam direction. ϕ is the azimuthal angle of the track.

[14] V. M. Abazov *et al.* (D0 Collaboration), The muon system of the Run II D0 detector, Nucl. Instrum. Methods Phys. Res., Sect. A **552,** 372 (2005).

[15] T. Aaltonen *et al.* (CDF Collaboration), Measurement of the $B_c^{\pm}$ production cross section in $p\bar{p}$ collisions at $\sqrt{s} = 1.96$ TeV, Phys. Rev. D **93,** 052001 (2016).

[16] S. Chatrchyan *et al.* (CMS Collaboration), J/ψ and $\psi(2S)$ production in pp collisions at $\sqrt{s} = 7$ TeV, J. High Energy Phys. 02 (2012) 011.

[17] T. Aaltonen *et al.* (CDF Collaboration), Production of $\psi(2S)$ mesons in $p\bar{p}$ collisions at $\sqrt{s} = 1.96$ TeV, Phys. Rev. D **80,** 031103 (2009).

[18] R. Aaij *et al.* (LHCb Collaboration), Measurement of $\psi(2S)$ production cross-section in proton-proton collisions at 7 and 13 TeV, Eur. Phys. J. C **80,** 485 (2020).

[19] A. Espositi *et al.*, The nature of $X(3872)$ from high-multiplicity pp collisions, arXiv:2006.15044.

[20] R. Aaij *et al.* (LHCb Collaboration), Observation of multiplicity-dependent prompt $\chi_{c1}(3872)$ and $\Psi(2S)$ production, arXiv:2009.06619.